Influences of excitation-dependent bandstructure changes on InGaN light-emitting diode efficiency

Weng W. Chow,*

(Dated: July 5, 2011)

Abstract

Bandstructure properties in wurtzite quantum wells can change appreciably with changing carrier density because of screening of quantum-confined Stark effect. An approach for incorporating these changes in an InGaN light-emitting-diode model is described. Bandstructure is computed for different carrier densities by solving Poisson and k·p equations in the envelop approximation. The information is used as input in a dynamical model for populations in momentum-resolved electron and hole states. Application of the approach is illustrated by modeling device internal quantum efficiency as a function of excitation.

PACS numbers: todo

Keywords: todo

INTRODUCTION

Considerable progress is being made in advancing InGaN light-emitting diodes (LEDs). However, there are still concerns involving performance limitations. An example is efficiency loss at high current density (efficiency droop) [1], which can limit use of LEDs in applications requiring intense illumination. Understanding and mitigating the efficiency droop mechanism is important. Several explanations have been proposed, including carrier leakage [2], Auger recombination [3], junction heating [4], carrier and defect delocalizations [5, 6]. The assertions are much debated. For example, in the case of Auger scattering, discrepancy exists in the Auger coefficient estimation between experimental-curve fitting and microscopic calculations [3, 7–9].

Discussions involving InGaN LED efficiency are commonly based on a rate equation for the total carrier density. The approach allows one to describe radiative and nonradiative carrier loss rates, where the latter typically includes ad-hoc terms for producing an efficiency droop. A particularly successful model, in terms of reproducing experimental efficiency versus injection current data, is the ABC model. [3, 7] The model's name derives from the three phenomenological constants (A, B and C) introduced to account for Shockley-Read-Hall (SRH), radiative-recombination and Auger-scattering carrier losses, respectively. Bandstructure effects enter indirectly via these coefficients.

It is known that the bandstructure in wurtzite quantum-well (QW) structures can change noticeably with carrier density because of screening of the quantum-confined Stark effect (QCSE) [10, 11]. Incorporating these changes into the ABC model is challenging, without compromising the attractiveness of having only three fitting parameters, each with direct correspondence to a physical mechanism. This paper considers an alternative that allows direct input of bandstructure properties, in particular, the band energy dispersions, confinement energies and optical transition matrix elements, as well as their carrier-density dependences arising from screening of piezoelectric and spontaneous polarization fields. The model has the further advantage of providing a consistent treatment of spontaneous emission, carrier capture and leakage, and nonequilibrium effects. Thus, the fitting parameter, B is eliminated and effects, such as plasma heating, are taken in account within an effective relaxation rate approximation for carrier-carrier and carrier-phonon scattering. All this is accomplished by extending a previously reported non-equilibrium LED model that is based

on dynamical equations for electron and hole occupations in each momentum (k) state [12]. The additions include an algorithm for simplifying and extracting bandstructure information relevant to the dynamical equations. Detailed bandstructure properties are obtained from solving $k \cdot p$ and Poisson equations [13]. Furthermore, since distinction between QW and barrier states is sometimes difficult in the presence of strong internal electric fields, extension is made to treat optical emission from these states on equal footing.

Section 2 describes the model, derivation of the working equations and calculation of input bandstructure properties. Section 3 demonstrates the application of the $k-$resolved model by calculating internal quantum efficiency (IQE) as a function of injection current for a multi-QW InGaN LED. Results are presented to illustrate IQE behavior that may be overlooked when not accounting for the excitation dependences of bandstructure. Most interesting is a possible contribution to efficiency droop from a change in relative emission contributions from QWs and barriers. Simulation results are presented to demonstrate the robustness of this mechanism to input parameter variations. Also in this section, a back-of-the-envelop derivation is used to associate the predicted droop to bandstructure changes from screening of QCSE. Section 4 further explains the bandstructure-induced droop mechanism by discussing the changes in QW confinement energies and envelop function overlap with increasing excitation. The section also presents a possible resolution to the discrepancy on the Auger coefficient estimation between ABC model and microscopic calculation. With the present model, the Auger coefficient necessary to maintain an efficiency droop at high injection current, as presently observed in experiments, is in the range of 5×10^{-32} to $10^{-31} cm^6 s^{-1}$, which is in closer agreement with microscopic calculations. Section 5 summarizes the paper.

THEORY

The following Hamiltonian, adapted from quantum optics [14], is used in the derivation of spontaneous emission from QW and barrier transitions:

$$H = \sum_i \varepsilon_i^e a_i^\dagger a_i + \sum_j \varepsilon_j^h b_j^\dagger b_j + \sum_q \hbar\Omega_q c_q^\dagger c_q - \sum_{i,j,q} \wp_{ij} \sqrt{\frac{\hbar\Omega_q}{V\epsilon_b}} (a_i b_j c_q^\dagger + c_q b_j^\dagger a_i^\dagger) \qquad (1)$$

The summations are over QW and barrier states with subscript $i(j)$ representing $e, \alpha_e, k_\perp$ $(h, \alpha_h, k_\perp)$ for QW states and e, k (h, k) for barrier states. In this notation, each QW state

is denoted by its charge σ, subband α_σ and in-plane momentum $k_\perp$. A bulk state is specified by its charge σ and 3-dimensional carrier momentum k. In Eq. (1), a_i,$a_i^\dagger$ (b_j,$b_j^\dagger$) are electron (hole) annihilation and creation operators, c_q, $c_q^\dagger$ are corresponding operators for the photons, ε_i^σ is the carrier energy, Ω_q is the photon frequency, $\wp_{ij}$ is the dipole matrix element, V is the active region volume and ϵ_b is the host permittivity. Using the Hiesenberg operator equations of motion and the above Hamiltonian, the carrier populations and polarizations evolve according to

$$\frac{\mathrm{d}\left\langle a_i^\dagger a_i\right\rangle}{\mathrm{d}t} = \cos i \sum_{j,q} \wp_{ij}\sqrt{\frac{\Omega_q}{\hbar V\epsilon_b}}\left[\left\langle c_q b_j^\dagger a_i^\dagger\right\rangle - \left\langle a_i b_j c_q^\dagger\right\rangle\right] \tag{2}$$

$$\frac{\mathrm{d}\left\langle b_j^\dagger b_j\right\rangle}{\mathrm{d}t} = i\sum_{i,q} \wp_{ij}\sqrt{\frac{\Omega_q}{\hbar V\epsilon_b}}\left[\left\langle c_q b_j^\dagger a_i^\dagger\right\rangle - \left\langle a_i b_j c_q^\dagger\right\rangle\right] \tag{3}$$

$$\begin{aligned}\frac{\mathrm{d}\left\langle a_i b_j c_q^\dagger\right\rangle}{\mathrm{d}t} &= -i\left(\Omega_q - \Omega_{ij}\right)\left\langle a_i b_j c_q^\dagger\right\rangle \\ &\quad + i\wp_{ij}\sqrt{\frac{\Omega_q}{\hbar V\epsilon_b}}\left\langle\left(a_i^\dagger a_i + b_j^\dagger b_j - 1\right)c_q^\dagger c_q + a_i^\dagger a_i b_j^\dagger b_j\right\rangle + ...\end{aligned} \tag{4}$$

where $\Omega_{ij} = \left(\varepsilon_i^e + \varepsilon_j^h\right)/\hbar$ is the transition frequency. Factorizing the operator products and truncating at the first level (Hartree-Fock approximation) give for Eq. (4)

$$\begin{aligned}\frac{\mathrm{d}\left\langle a_i b_j c_q^\dagger\right\rangle}{\mathrm{d}t} &= i\left(\Omega_q - \Omega_{ij}\right)\left\langle a_i b_j c_q^\dagger\right\rangle \\ &\quad - i\wp_{ij}\sqrt{\frac{\Omega_q}{\hbar V\epsilon_b}}\left[\left(\left\langle a_i^\dagger a_i\right\rangle + \left\langle b_j^\dagger b_j\right\rangle - 1\right)\left\langle c_q^\dagger c_q\right\rangle + \left\langle a_i^\dagger a_i\right\rangle\left\langle b_j^\dagger b_j\right\rangle\right]\end{aligned} \tag{5}$$

For an LED, it is customary to assumed that cavity influence is sufficiently weak so that $\left\langle c_q^\dagger c_q\right\rangle << 1$ and only the spontaneous emission contribution is kept. Additionally, polarization dephasing is introduced, where the dephasing (with coefficient γ) is assumed to be considerably faster than the population changes. This allows integration of Eq. (5). The result is used to eliminate the polarization in Eqs. (2) and (3), giving

$$\frac{\mathrm{d}\left\langle a_i^\dagger a_i\right\rangle}{\mathrm{d}t} = -\left\langle a_i^\dagger a_i\right\rangle\sum_{j,q}\frac{2\Omega_q}{\hbar\epsilon_b V\gamma}\left|\wp_{ij}\right|^2\left\langle b_j^\dagger b_j\right\rangle\left[1+\left(\frac{\Omega_{ij}-\Omega_q}{\gamma}\right)^2\right]^{-1} \tag{6}$$

$$\frac{\mathrm{d}\left\langle b_j^\dagger b_j\right\rangle}{\mathrm{d}t} = -\left\langle b_j^\dagger b_j\right\rangle\sum_{i,q}\frac{2\Omega_q}{\hbar\epsilon_b V\gamma}\left|\wp_{ij}\right|^2\left\langle a_i^\dagger a_i\right\rangle\left[1+\left(\frac{\Omega_{ij}-\Omega_q}{\gamma}\right)^2\right]^{-1} \tag{7}$$

Converting the photon momentum summation into an integral, i.e.

$$\sum_q \rightarrow 2\frac{V}{(2\pi)^3}\int_0^\infty \mathrm{d}q\ 4\pi q^2 \tag{8}$$

where $\Omega_q = qc$ and c is the speed of light in the semiconductor, the right-hand sides of Eqs. (6) and (7) may be integrated to give

$$\frac{\mathrm{d}\left\langle a_i^\dagger a_i\right\rangle}{\mathrm{d}t} = -\left\langle a_i^\dagger a_i\right\rangle \sum_j \frac{n_b}{\hbar\epsilon_0\pi c^3}\left|\wp_{ij}\right|^2\Omega_{ij}^3\left\langle b_j^\dagger b_j\right\rangle \tag{9}$$

$$\frac{\mathrm{d}\left\langle b_j^\dagger b_j\right\rangle}{\mathrm{d}t} = -\left\langle b_j^\dagger b_j\right\rangle \sum_i \frac{n_b}{\hbar\epsilon_0\pi c^3}\left|\wp_{ij}\right|^2\Omega_{ij}^3\left\langle a_i^\dagger a_i\right\rangle \tag{10}$$

Writing explicitly for QW populations and adding phenomenologically SRH carrier loss and relaxation contributions from carrier-carrier and carrier-phonon scattering, gives

$$\begin{aligned}\frac{\mathrm{d}n_{\sigma,\alpha_\sigma,k_\perp}}{\mathrm{d}t} = & -n_{\sigma,n_\sigma,k_\perp}\sum_{\alpha_{\sigma'}} b_{\alpha_\sigma,\alpha_{\sigma'},k_\perp}n_{\sigma',\alpha_{\sigma'},k_\perp} - An_{\sigma,n_\sigma,k_\perp} \\ & -\gamma_{c-c}\left[n_{\sigma,n_\sigma,k_\perp} - f\left(\varepsilon_{\sigma,k_\perp},\mu_\sigma,T\right)\right] \\ & -\gamma_{c-p}\left[n_{\sigma,n_\sigma,k_\perp} - f\left(\varepsilon_{\sigma,k_\perp},\mu_\sigma^L,T_L\right)\right]\end{aligned} \tag{11}$$

where σ,σ' is e,h or h,e. In Eq. (11), γ_{c-c} and γ_{c-p} are the effective carrier-carrier and carrier-phonon collision rates, respectively, and

$$b_{\alpha_\sigma,\alpha_{\sigma'},k_\perp} = \frac{1}{\hbar\epsilon_b\pi c^3}\left|\wp_{\alpha_\sigma,\alpha_{\sigma'},k_\perp}\right|^2\Omega_{\alpha_\sigma,\alpha_{\sigma'},k_\perp}^3 \tag{12}$$

where $\wp_{\alpha_\sigma,\alpha_{\sigma'},k_\perp}$ and $\Omega_{\alpha_\sigma,\alpha_{\sigma'},k_\perp}$ are the QW dipole matrix element and transition energy. Similarly, for the barrier populations,

$$\begin{aligned}\frac{\mathrm{d}n_{\sigma,k}^b}{\mathrm{d}t} = & -b_k n_{e,k}^b n_{h,k}^b + \frac{J}{eN_\sigma^p}f\left(\varepsilon_{\sigma,k}^b,\mu_\sigma^p,T_p\right)\left(1-n_{\sigma,k}^b\right) - \gamma_b n_{\sigma,k} \\ & -\gamma_{c-c}\left[n_{\sigma,k}^b - f\left(\varepsilon_{\sigma,k}^b,\mu_\sigma,T\right)\right] \\ & -\gamma_{c-p}\left[n_{\sigma,k}^b - f\left(\varepsilon_{\sigma,k}^b,\mu_\sigma^L,T_L\right)\right]\end{aligned} \tag{13}$$

where

$$b_k = \frac{1}{\hbar\epsilon_b\pi c^3}\left|\wp_k\right|^2\Omega_k^3, \tag{14}$$

$\wp_k$ and Ω_k are the barrier dipole matrix element and transition energy. In Eq. (13) is a pump contribution, where J is the current density, e is the electron charge, $N_\sigma^p = \sum_k f\left(\varepsilon_{\sigma,k}^b, \mu_\sigma^p, T_p\right)$ and $f\left(\varepsilon_{\sigma,k}^b, \mu_\sigma^p, T_p\right)$, the injected carrier distribution, is a Fermi-Dirac function with chemical potential μ_σ^p and temperature T_p. For the asymptotic Fermi-Dirac distributions approached via carrier-carrier collisions, the chemical potential μ_σ and plasma temperature T are determined by conservation of carrier density and energy. In the case of carrier-phonon collisions, the chemical potential μ_σ^L is determined by conservation of carrier density and the lattice temperature T_L is an input quantity. Total carrier density and energy are computed by converting the sum over states to integrals, i.e.,

$$\sum_{k_\perp} \rightarrow \frac{S}{(2\pi)^2} 2 \int_0^\infty \mathrm{d}k_\perp \; 2\pi k_\perp \quad \text{and} \quad \sum_k \rightarrow \frac{hS}{(2\pi)^3} 2 \int_0^\infty \mathrm{d}k \; 4\pi k^2 \tag{15}$$

where S and h are the surface area and thickness of the active active region consisting of all QW and barrier layers. Further details involving implementation and comparison with results from quantum-kinetic calculations are reported elsewhere [15, 16]. Many-body effects [17, 18] are neglected in Eqs (11) and (13). Their incorporation, at least at the level of the screened Hartree-Fock approximation [15], will be considered in future investigations.

Bandstructure information enters directly into Eqs (11) and (13) via the dipole matrix elements $\wp_{\alpha_\sigma,\alpha_{\sigma'},k_\perp}$, $\wp_k$ and carrier energies $\varepsilon_{\sigma,k_\perp}$, $\varepsilon_{\sigma,k}^b$. From $k \cdot p$ theory, the QW electron and hole eigenfunctions are [18]

$$\langle r \left| \phi_{\sigma,\alpha_\sigma,k_\perp} \right\rangle = e^{ik_\perp \cdot r_\perp} \sum_{m_\sigma} \sum_{\beta_\sigma} A_{\beta_\sigma,\alpha_\sigma,k_\perp} u_{m_\sigma,\beta_\sigma}(z) \langle r \left| m_\sigma \right\rangle \tag{16}$$

where $|m_\sigma\rangle$ is a bulk electron or hole state, $u_{m_\sigma,\beta_\sigma}(z)$ is the β_σ-th envelop function associated with the m_σ bulk state, $A_{\beta_\sigma,\alpha_\sigma,k_\perp}$ is the amplitude of the β_σ-th envelop function contributing to the α_σ-th subband at momentum $k_\perp$, z is position in the growth direction and $r_\perp$ is position in the QW plane Using Eq. (16), the square of the dipole matrix element may then be written as

$$\begin{aligned} \left|\wp_{\alpha_e,\alpha_h,k_\perp}\right|^2 &\equiv \left|\langle \phi_{e,\alpha_e,k_\perp} \left| ex \right| \phi_{h,\alpha_h,k_\perp} \rangle\right|^2 \\ &= \left|\wp_{bulk}\right|^2 \xi_{\alpha_e,\alpha_h,k_\perp} \end{aligned} \tag{17}$$

where

$$\xi_{\alpha_e,\alpha_h,k_\perp} = \frac{1}{4}\left|\sum_{\beta_e}\sum_{\beta_h}\sum_{m_e}\sum_{m_h} A_{\beta_e,\alpha_e,k_\perp} A_{\beta_h,\alpha_h,k_\perp} \times \int_{-\infty}^{\infty} dz\; u_{m_e,\beta_e}(z) u_{m_h,\beta_e}(z)\right|^2 \tag{18}$$

and the bulk dipole matrix element in the absence of an electric field is given by

$$|\wp_{bulk}|^2 = \frac{\hbar^2}{2m_0\varepsilon_g}\left(\frac{m_0}{m_e}-1\right)\left(1+\frac{\Delta_1+\Delta_2}{\varepsilon_g}\right), \tag{19}$$

ε_g is the bulk material bandgap energy, m_0 and m_e are the bare and effective electron masses, Δ_1 and Δ_2 are energy splittings associated with the bulk hole states. An iterative solution of the $k\cdot p$ and Poisson equations [13] is used to obtain the energies $\varepsilon_{\sigma,\alpha_\sigma,k_\perp}$ and $\varepsilon^b_{\sigma,k}$ and the overlap integral $\xi_{\alpha_e,\alpha_h,k_\perp}$. For these calculations we use the the bulk wurtzite material parameters listed in Refs. [19–22].

RESULTS

With the present model, it is necessary to solve the bandstructure and population problems self consistently. Simultaneous solution of both problems is very challenging and perhaps unnecessary. The approach used in this paper is to first take care of the bandstructure part by iteratively solving the $k\cdot p$ and Poisson equations for a range of carrier densities. Bandstructure information needed for the population part are $\varepsilon_{\sigma,\alpha_\sigma,k_\perp}$, $\varepsilon^b_{\sigma,k}$ and $\xi_{\alpha_e,\alpha_h,k_\perp}$ versus total QW carrier density, $n^{qw}_\sigma = S^{-1}\sum_{\alpha_\sigma,,k_\perp} n_{\sigma,\alpha_\sigma,k_\perp}$, where the n^{qw}_σ dependences are from screening of the QW electric field.

To facilitate the solution of the dynamical population equations, the carrier states are grouped into two categories: those belonging to the QWs and those belonging to the barriers. The QW states are treated using Eq. (11) and the barrier states are treated collectively with Eq. (13). With a high internal electric field, the distinction between QW and barrier states may be ambiguous. In this paper, the choice is made by calculating $\int_{QW}\mathrm{dz}\;|u_{m_\sigma,\beta_\sigma}(z)|^2$, where integral is performed over the QWs. The states where the integral is greater than a half are grouped as QW states and the rest as barrier states. For the problem being addressed, which is the excitation dependence of IQE, the distinction is only important because only QW transitions are affected by QCSE. For the barrier transitions, the dipole

matrix element in the presence of an internal electric field is approximated by an average, where each transition is weighted according to the occupations of the participating states. When solving the population equations, grouping the barrier states appreciably reduces numerical demand, which remains substantial because one is still keeping track of a large number of k-states.

The second step involves numerically solving Eqs. (11) and (13) with the bandstructure quantities updated at each time step according to the instantaneous value of n_σ^{qw}. When steady state is reached, IQE is obtained from dividing the rate of carrier (electron or hole) loss via spontaneous emission by the rate of carrier injection:

$$IQE = \frac{e}{JS}\left(\sum_{\alpha_e,\alpha_h,k_\perp} b_{\alpha_e,\alpha_h,k_\perp} n_{e,\alpha_e,k_\perp} n_{h,\alpha_h,k_\perp} + \sum_k b_k n_{e,k}^b n_{h,k}^b\right) \tag{20}$$

Computed IQE versus current density curves for different SRH coefficients in the QWs are plotted in Fig. 1. Each curve shows an initial sharp increase in IQE with injection current, with emission occurring the instant there is an injected current. Quite interesting, especially because Auger carrier loss is not included in the model, is the appearance of efficiency droop in the curves for high A values. A higher SRH coefficient in QW than barrier is possible in present experimental devices, based on the roughly three times higher defect density in QWs than in barriers in LEDs measured at Sandia [23]. The calculations are performed assuming an active region consisting five 4nm $In_{0.2}Ga_{0.8}N$ QWs separated by 6nm GaN barriers and bounded by 20nm GaN layers. Electric field in the QWs is determined from the sum of piezoelectric and spontaneous polarization fields. The electric fields in the barriers are from spontaneous polarization. Screening of these fields are determined semiclassically according to Poisson equation, and electron and hole envelop functions. Input parameters are $A_b = 10^7 s^{-1}$, $T_L = 300K$, $\gamma_{c-c} = 5 \times 10^{13} s^{-1}$ and $\gamma_{c-p} = 10^{13} s^{-1}$. Effects arising from doping profile and presence of carrier blocking layers are ignored.

To uncover the mechanism giving rise to the droop behavior shown in Fig. 1, it may be more effective to use a less comprehensive model to isolate bandstructure effects by ignoring carrier leakage and nonequilibrium effects. Such a model is possible by extending the ABC model to distinguish between QW and barrier carrier densities, N_σ and N_σ^b, respectively. The following phenomenological (and less rigorous than Eqs .(11) and (13)] rate equations

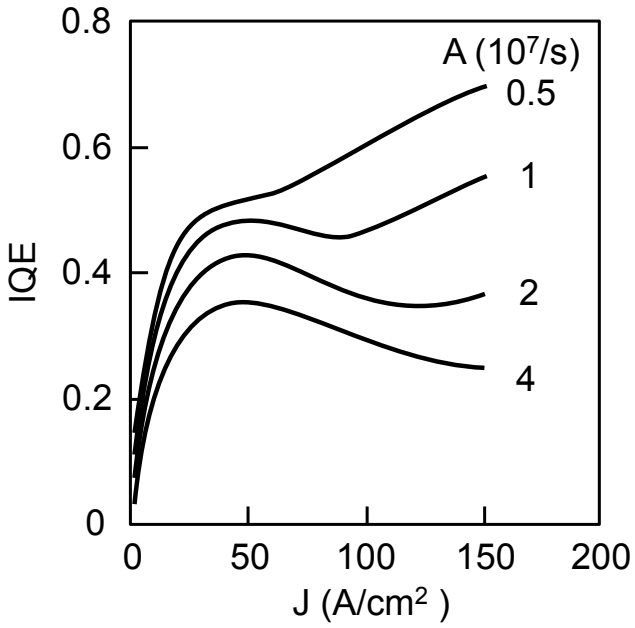

Figure 1: Internal quantum efficiency versus current density for different QW SRH coefficients. The curves are computed using the $k-$resolved model described by Eqs. (11) and (13) for a LED with a $In_{0.2}Ga_{0.8}N/GaN$ multi-QW active region (see Fig. 4).

may be written:

$$\frac{\mathrm{d}N_\sigma}{\mathrm{d}t} = -BN_eN_h - AN_\sigma \tag{21}$$

$$\frac{\mathrm{d}N_\sigma^b}{\mathrm{d}t} = -B_bN_e^bN_h^b - A_bN_\sigma^b + \frac{J}{eh_b} \tag{22}$$

where $\sigma = e$ or h. 3-d (volume) densities are used to connect with the ABC model, especially in terms of the SRH and spontaneous emission coefficients. Equations (21) and (22) are coupled by assuming that intraband collisions are sufficiently rapid so that QW and barrier populations are in equilibrium at temperature T. Defining a total 2-d carrier density, $N_{2d} = N_{qw}hN_\sigma + h_bN_\sigma^b$ allows combining these equations to give

$$\frac{\mathrm{d}N_{2d}}{\mathrm{d}t} = -\beta N_{2d}^2 - A_bN_{2d} + \frac{J}{e} \tag{23}$$

where N_{qw} is the number of QWs in the structure, h is the width of individual QWs,

$$\beta = \frac{\frac{h}{h_b}N_{qw}B + B_b\exp\left(\frac{\Delta_e+\Delta_h}{k_BT}\right)}{\left[1+\exp\left(\frac{\Delta_e}{k_BT}\right)\right]\left[1+\exp\left(\frac{\Delta_h}{k_BT}\right)\right]} \tag{24}$$

k_B is Boltzmann constant and Δ_σ is the averaged QW confinement energy. The steady state solution to Eq. (23) gives the internal quantum efficiency,

$$IQE = \frac{\beta N_{2d}^2}{J/e} = 1 - 2\frac{J_0}{J}\left[\sqrt{\frac{J}{J_0}+1} - 1\right] \tag{25}$$

where $J_0 = e\gamma_b^2\,(4\beta)^{-1}$ and $A/A_b = N_{qw}h/h_b$ is assumed to simplify the above expressions.

Bandstructure input to Eq. (25) are the confinement energies Δ_e, Δ_h and the QW B coefficient as functions of total carrier density, N_{2d}. The information is extracted from the same bandstructure calculations performed for the more comprehensive $k-$resolved model, with the exception that only the zone center ($k_\perp = k = 0$) values are used. Confinement energies are approximated by $\Delta_\sigma = \langle\varepsilon_{\sigma,\alpha_\sigma,0}\rangle_{QW} - \varepsilon^b_{\sigma,0}$, where $\langle\rangle_{QW}$ indicates an average over QW states. Based on Eqs. (12), (14) and (17), the assumption $B = \langle\xi_{\alpha_e,\alpha_h,0}\rangle_{QW}\,\eta B_b$ is made, where $\langle\xi_{\alpha_e,\alpha_h,0}\rangle_{QW}$ is the average envelop function overlap of the allowed QW transitions and η is introduced to account for the difference in QW and barrier densities of states. This difference is automatically taken care of in the $k-$resolved model based on Eqs. (11) and (13). Δ_e, Δ_h and $\langle\xi_{\alpha_e,\alpha_h,0}\rangle_{QW}$ versus carrier density N_{2d} are plotted in Fig. 2. The sheet (2-d) density N_{2d} is for a heterostructure consisting 5 QWs and 6 barrier layers that totals 84nm in width.

Figure 3 shows IQE versus current density computed with Eq. (25) and for different η. Input parameters are $T = 300K$, $N_{qw}h/h_b = 0.16$ and $A_b^2/B_b = 1.1\times10^{24}cm^{-3}s^{-1}$. All the curves depict pronounced efficiency droop from the extended ABC model, where carrier dependences of confinement energies and QW bimolecular radiative coefficient are taken into account. They also indicate that the appearance of droop is insensitive to the fitting parameter η, which affects only the IQE recovery arising from increase in QW emission.

While the above exercise reveals that bandstructure changes is the source of droop, differences between Figs. 1 and 2 suggest that there is also influence from other contributions. That experimental results are in closer agreement with Fig. 1 indicates the importance of these contributions in present LEDs. They include energy dispersions, carrier leakage and nonequilibrium carrier effects, such as an incomplete transfer of the carrier population from barrier to QW states because of finite intraband collision rates. The presence of nonequilibrium effects is verified from least-squares fits of computed carrier populations to Fermi-Dirac distributions. For $J = 150A/cm^2$, the fits indicate elevated plasma temperatures of $T > 360K$ for carrier-phonon scattering rate $\gamma_{c-p} = 10^{13}s^{-1}$ and $T > 600K$ for

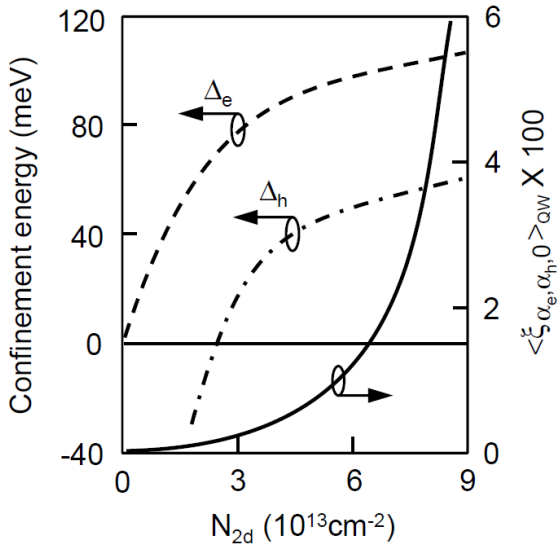

Figure 2: Average QW confinement energies (left axis) and electron-hole wavefunction overlap (right axis) versus carrier density. The curves are extracted from solving $k\cdot p$ and Poisson equations. A negative average hole confinement energy is possible because of the tilt in QW confinement potential and the presence of states in the outer barrier regions cladding the QWs, as shown in Fig. 4(a).

$\gamma_{c-p} = 10^{12}s^{-1}$.

Lastly, the dynamical solution gives the carrier densities in QW and barrier states. The conversion to bulk (3-d) density is via division by the total QW layer width $N_{qw}h$ in the case of the QW and by the total barrier width h_b in the case of the barrier. When performing the bandstructure calculation, quasiequilibrium condition is assumed to determine the QW and barrier bulk densities used in the solution of Poisson equation. This is an inconsistency that is acceptable provided the dynamical solution does not produce carrier distributions deviating too far from quasiequilibrium distributions. Even though the current density versus carrier density relationship depends on the input to the dynamical problem, and therefore, different for the different curves in Fig. 1, some insight into the connection between bandstructure and IQE excitation dependence may be obtained by examining Figs. 1 and 2 together. The onset of droop in the curves in Fig. 1 occurs around $45A/cm^2$, which corresponds to N_{2d} around $10^{13}cm^{-2}$ or a 3-d QW carrier density of $1\times$ to $1.2\times10^{18}cm^{-3}$. At these densities, the QCSE is essentially unscreened. At the start of IQE recovery which occurs over the range of

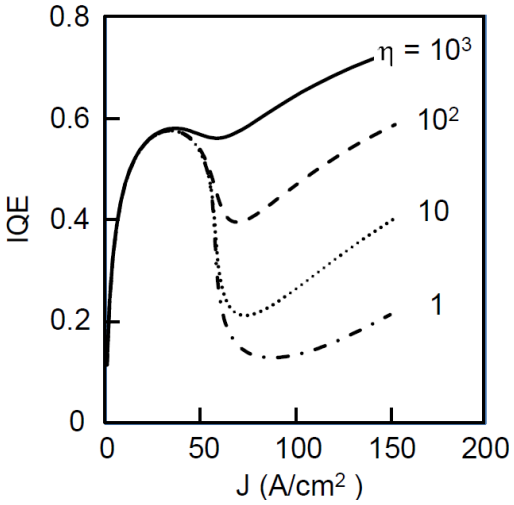

Figure 3: Internal quantum efficiency versus current density computed using Eq. (25) from an extended ABC model. The model isolates the bandstructure-induced droop mechanism. The curves are for different η, a free parameter accounting for difference between QW and barrier bimolecular radiative recombination coefficients (B and B_b, respectively) because of differences in densities of state.

60 to $120 A/cm^2$, the corresponding carrier densities are $2.8 \times 10^{13} < N_{2d} < 3.0 \times 10^{13} cm^{-2}$ or 3-d QW carrier density of $8.5\times$ to $9 \times 10^{18} cm^{-2}$. According to Fig. 2, these are densities where wavefunction overlap is no longer negligible. Between the IQE peak and recovery, N_{2d} changes from approximately 10^{13} to $3.0 \times 10^{13} cm^{-2}$. Within that carrier density range, Fig. 2 shows significant increase in QW-barrier electron and hole energy separations.

DISCUSSION OF RESULTS

Further insight into the bandstructure-induced droop mechanism is possible from closer examination of the bandstructure changes with excitation. Figure 4 shows the absolute square of electron and hole envelop functions at zone center ($k_\perp = k = 0$) for four different carrier densities. For clarity, the curves are separated vertically according to their associated energies. The black lines plot the electron and hole confinement potentials, while the red and blue curves indicate the QW and barrier states, respectively.

Starting at a carrier density of $N_{2d} = 2.3 \times 10^{13} cm^{-2}$, Fig. 4(a) depicts confinement potentials differing appreciably from the flat-band situation [see Fig. 4(d)]. A result is small

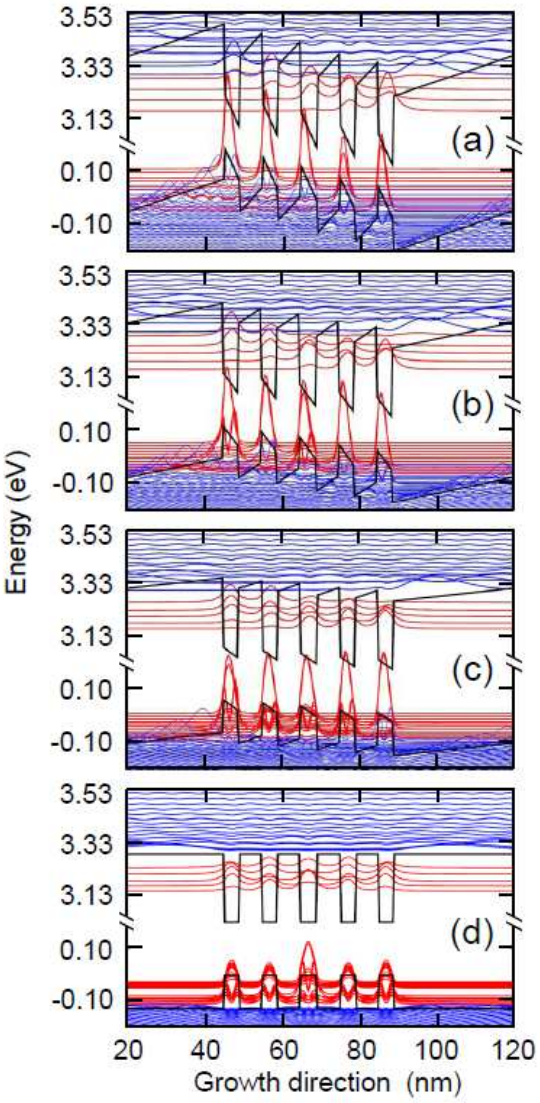

Figure 4: Absolute square of envelop functions for electrons and holes for carrier densities, N_{2d} = (a) 2.25×, (b) 3.47× and (c) $6.89 \times 10^{13} cm^{-2}$. Figure 4(d) is the flat-band limit. Each curve is displaced according to its bandedge energy for clarity. Envelop functions belonging to QW and barrier states are indicated by red and blue curves, respectively. The black lines plot the confinement potentials. The x-axis is along the growth direction.

energy separation between QW and barrier states, leading to comparable QW and barrier populations, especially for the holes. Optical emission from barrier transitions occur via the contribution $\sum_k b_k n^b_{e,k} n^b_{h,k}$, as soon as the product of electron and hole populations, $n^b_{e,k} n^b_{h,k}$ becomes nonzero. In contrast, the QW contribution $\sum_{\alpha_e,\alpha_h,k_\perp} b_{\alpha_e,\alpha_h,k_\perp} n_{e,\alpha_e,k_\perp} n_{h,\alpha_h,k_\perp}$ is

negligible, even though the product $n_{e,\alpha_e,k\perp}n_{h,\alpha_h,k\perp}$ may be appreciable. This is because QCSE spatially separates electrons and holes in the QWs, resulting in very small dipole matrix elements for QW transitions.

At a higher carrier density of $N_{2d} = 3.4\times10^{13}cm^{-2}$, increased screening of QCSE leads to higher energy separation between QW and barrier states as shown in Fig. 4(b). This causes the barrier populations to decrease relative to those of the QW. However, the QCSE is still sufficient to suppress the dipole matrix element. The net result is reduced IQE because the smaller increase in $\sum_k b_k n^b_{e,k} n^b_{h,k}$ with increasing excitation that is not compensated by a corresponding increase in $\sum_{\alpha_e,\alpha_h,k_\perp} b_{\alpha_e,\alpha_h,k_\perp} n_{e,\alpha_e,k_\perp} n_{h,\alpha_h,k_\perp}$. Important to the appearance of droop is a lag between the increase in confinement energies and the increase in QW dipole matrix element, as illustrated in Fig. 2 within the region $2.5\times10^{13}cm^{-2} < N_{2d} < 5\times10^{13}cm^{-2}$.

For the increase in QW emission, a high carrier density is necessary to sufficiently screen the QW electric field. That is the case for Fig. 4(c), where $N = 6.8\times10^{13}cm^{-2}$. An appreciable QW emission leads to a reversal of the IQE droop as shown in Figs. 1 and 3. Lastly, Fig. 4(d) shows the asymptotic flat-band case, both for reference and as a guide for assigning QW and barrier states. Note that some ambiguity remains, especially with the $n = 2$ subbands, which lie mostly in the triangular barrier regions of the confinement potentials at finite carrier densities.

Questions remain concerning the bandstructure-induced droop mechanism. For example, one might expect a significant red shift of emission energy when optical transitions changes from barrier dominated to QW dominated. This need not be the case because of the energy level shifts associated with the QCSE and Franz-Keldysh effects [24].

The curves in Fig. 5 show the carrier density dependences of the average QW and barrier bandedges, $\langle\varepsilon_{e,\alpha_e,0}\rangle_{QW} + \langle\varepsilon_{h,\alpha_h,0}\rangle_{QW}$ and $\varepsilon^b_{e,0} + \varepsilon^b_{h,0}$, respectively. To a good approximation, emission energy is centered around the lower of the curves, which means that except for slight deviations around the cross-over region, the emission energy is blue shifted with increasing excitation. Furthermore, it is always below the zero-field barrier bandgap.

Another question concerns the curves depicting IQE recovery at current densities lower than observed in present experiments. This discrepancy suggests the presence of other loss mechanisms, such as Auger carrier loss.

To illustrate the effect of Auger scattering, Auger carrier loss is incorporated into Eqs.

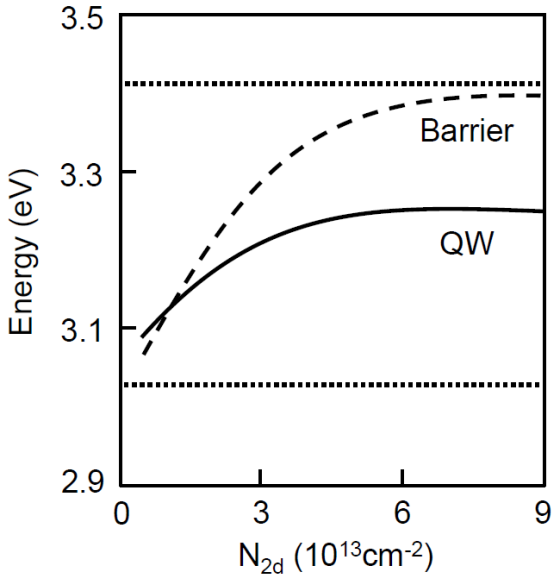

Figure 5: Average QW and barrier bandedge energies (solid and dashed curves, respectively) versus carrier density. Optical emission should be centered approximately at the lower of the 2 curves. The upper and lower dotted lines indicate the strained-InGaN and unstrained-GaN bulk bandgap energies.

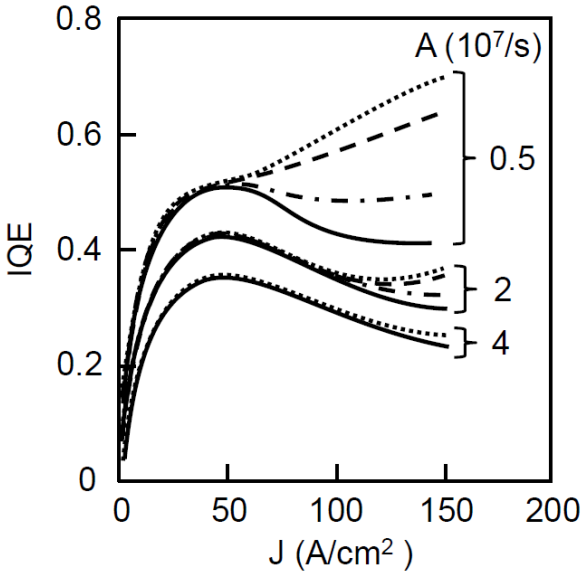

Figure 6: Internal quantum efficiency versus current density showing the influence of Auger carrier loss for different QW SRH coefficients. The Auger coefficients are $C = 0$, 10^{-32}, 5×10^{-32} and $10^{-31} cm^6 s^{-1}$ (dotted, dashed, dot-dashed and solid curves, respectively).

(11) and (13), as described in Ref. [12], and the results are shown in Fig. 6 for $A/A_b = 0.5$, 2 and 4, with Auger coefficient $C = 0$, 10^{-32}, 5×10^{-32} and $10^{-31} cm^6 s^{-1}$ (dotted, dashed, dot-dashed and solid curves, respectively). For clarity, the $A/A_b = 1$ case in Fig. 1 is omitted. The curves shows the prolonging of the efficiency droop by Auger carrier loss. More importantly, the necessary Auger coefficient is shown to be $C \gtrsim 5 \times 10^{-32} cm^6 s^{-1}$ which is appreciably smaller than that used in ABC models and are within the range predicted by microscopic calculation [9].

SUMMARY

This paper describes an approach to modeling InGaN LEDs that involves the self-consistent solution of bandstructure and carrier population problems. The motivation is to provide direct input of bandstructure properties, in particular, their carrier-density dependences arising from screening of piezoelectric and spontaneous polarization fields. Other advantages include consistent treatment of spontaneous emission, carrier capture and leakage and nonequilibrium effects, as well as description of optical emission from quantum-well and barrier transitions on equal footing.

The approach is applied to investigate the internal quantum efficiency as a function of injection current for a multi-QW InGaN LED. Among the behaviors that result from taking into account the excitation dependences of bandstructure, is a possible contribution to efficiency droop. Simulations performed with different sets of input parameter values show robustness of this mechanism. A simple, back-of-the-envelop derivation is used to trace the droop mechanism to bandstructure changes from screening of the quantum-confined Stark effect. Basically, the initial IQE peak has emission contribution from barrier states. The droop is caused by carrier transfer from these barrier states to QW states, where emission strength is weaker because the quantum-confined Stark effect remains largely unscreened.

Lastly, the results presented in this paper should not be generalized to imply that bandstructure effects are responsible for the entire droop phenomenon in all experiments. In fact, simulation results are presented to demonstrate the importance of other contributions, both intrinsic and extrinsic, for describing present IQE experiments. It is possible that the differences in observed droop behavior (involving different LED emitting wavelengths, polar versus non polar substrates, with or without electron blocking layers, etc.) arise from

differences in the relative importance of various mechanisms. The k-resolved LED model described in this paper can provide a more accurate estimation of their relative strengths. Furthermore, as shown in Sec. 4 for Auger loss, the model can also put arguments drawn from experimental-curve fitting on firmer ground by providing better connection to first-principles theory.

Acknowledgement

This work is performed at Sandia's Solid-State Lighting Science Center, an Energy Frontier Research Center (EFRC) funded by the U. S. Department of Energy, Office of Science, Office of Basic Energy Sciences. The author thanks A. Armstrong, M. Crawford, P. Smowton and J. Tsao for helpful discussions.

---

* Electronic address: wwchow@sandia.gov

[1] M.R. Krames, O.B. Shchekin, R. Mueller-Mach, G.O. Mueller, L. Zhou, G. Harbers and M. G. Craford, "Status and future of high-power light-emitting diodes for solid-state lighting," J. Display Technology **3**, 160-175 (2007).

[2] M. H. Kim, M. F. Schubert, Q. Dai, J. K. Kim, E. F. Schubert, J. Piprek, and Y. Park, "Origin of efficiency droop in GaN-based light-emitting diodes," Appl. Phys. Lett. **91**, 183507-183510 (2007).

[3] Y.C. Shen, G.O. Müller, S. Watanabe, N.F. Gardner, A. Munkholm and M.R. Krames, "Auger recombination in InGaN measured by photoluminescence," Appl. Phys. Lett. **91**, 141101-141101 (2007).

[4] A. A. Efremov, N. I. Bochkareva, R. I. Gorbunov, D. A. Larinvovich, Yu. T. Rebane, D. V. Tarkhin and Yu. G. Shreter, "Effect of the joule heating on the quantum efficiency and choice of thermal conditions for high-power blue InGaN/GaN LEDs," Semiconductors **40**, 605 (2006).

[5] S. F. Chichibu, T. Azuhata, M. Sugiyama, T. Kitamura, Y. Ishida, H. Okumurac, H. Nakanishi, T. Sota and T. Mukai, "Optical and structural studies in InGaN quantum well structure laser diodes," J. Vac, Sci. Technol. B **19**, 2177 (2001).

[6] J. Hader, J.V. Moloney and S.W. Koch, "Density-activated defect recombination as a possible explanation for the efficiency droop in GaN-based diodes," Appl. Phys. Lett. **96**, 221106-

221108 (2010).

[7] H.-Y Ryu, H.-S. Kim and J.-I. Shim, "Rate equation analysis of efficiency droop in InGaN light-emitting diodes," Appl. Phys. Lett. **95**, 081114-081117 (2009).

[8] J. Hader, J.V. Moloney, B. Pasenow, S.W. Koch, M. Sabathil, N. Linder and S. Lutgen, "On the important of radiative and Auger losses in GaN-based quantum wells," Appl. Phys. Lett. **92**, 261103-261105 (2008).

[9] K.T. Dellaney, P. Rinke and C.G. Van de Walle, "Auger recombination rates in nitrides from first principles," Appl. Phys. Lett. **94**, 191109-191111 (2009).

[10] A. Bykhovshi, B. Gelmonst and M. Shur, "The influence of the strain-induced electric field on the charge distribution in GaN-AlN-GaN structure," J. Appl. Phys. **74**, 6734-6739 (1993).

[11] J. S. Im, H. Kollmer, J. Off, A. Sohmer, F. Scholz and A. Hangleiter, "Reduction of oscillator strength due to piezoelectric fields in GaN/AlGaN quantum wells," Phys. Rev. B **57**, R9435-R9438 (1998).

[12] W. W. Chow, M. H. Crawford, J. Y. Tsao and M. Kneissl, "Internal efficiency of InGaN light-emitting diodes: Beyond a quasiequilibrium model," Appl. Phys. Lett. **97**, 121105-121107 (2010).

[13] S. L. Chuang and C. S. Chang, "$k \cdot p$ method for strained wurtzite semiconductors," Phys. Rev. B **54**, 2491-2504 (1996).

[14] E. Jaynes and F. Cummings, "Comparison of quantum and semiclassical radiation theories with application to the beam maser*Proc. IEEE **51**, 89-109 (1963).

[15] W.W. Chow, H.C. Schneider, S.W. Koch, C.H. Chang, L. Chrostowski and C. J. Chang-Hasnain, "Nonequilibrium model for semiconductor laser modulation response," IEEE Journ. Quantum Electron. **38**, 402 (2002).

[16] I. Waldmueller, W. W. Chow, M. C. Wanke and E. W. Young, "Non-equilibrium many-body theory of intersubband lasers," IEEE Journ. Quantum Electron. **42**, 292-301 (2006).

[17] W. W. Chow, A. F. Wright, A. Girndt, F. Jahnke and S. W. Koch, "Microscopic theory of gain for an InGaN/AlGaN quantum well laser," Appl. Phys. Lett. **71**, 2608-2610 (1997).

[18] W. W. Chow and S. W. Koch, *Semiconductor-Laser Fundamentals: Physics of the Gain Materials* (Springer, Berlin, 1999).

[19] S. J. Jenkins, g. P. Srivastava and J. C. Inkson, "Simple approach to self-energy corrections in semiconductors and insulators," Phys. Rev. B **48**, 4388 (1993).

[20] A. F. Wright and J. S. Nelson, "Consistent structural properties for AlN, GaN, and InN," Phys. Rev. B **51**, 7866-7869 (1995).

[21] S. H. Wei and A. Zunger, "Valence band splittings and band offsets of AlN, GaN, and InN," Appl. Phys. Lett. **69**, 2719-2711 (1996).

[22] O. Ambacher, "Growth and applications of Group III-nitrides," J. Phys. D: Appl. Phys. **31**, 2653-2710 (1998).

[23] A. Armstrong, Sandia National Laboratories, Albuquerque, NM 87185 (personal communication, 2010).

[24] L. V. Keldysh, "Behaviour of non-metallic crystals in strong electric fields,," Soviet Physics JETP **6,** 763-770 (1958).